Comparison between lidar and nephelometer measurements of aerosol hygroscopicity at the Southern Great Plains Atmospheric Radiation Measurement site

M. Pahlow,[1,2] G. Feingold,[1] A. Jefferson,[3] E. Andrews,[3] J. A. Ogren,[3] J. Wang,[4] Y.-N. Lee,[4] R. A. Ferrare,[5] and D. D. Turner[6]

Received 30 November 2004; revised 6 May 2005; accepted 24 June 2005; published 28 January 2006.

[1] Aerosol hygroscopicity has a significant effect on radiative properties of aerosols. Here a lidar method, applicable to cloud-capped, well-mixed atmospheric boundary layers, is employed to determine the hygroscopic growth factor *f*(RH) under unperturbed, ambient atmospheric conditions. The data used for the analysis were collected under a wide range of atmospheric aerosol levels during both routine measurement periods and during the intensive operations period (IOP) in May 2003 at the Southern Great Plains (SGP) Climate Research Facility in Oklahoma, USA, as part of the Atmospheric Radiation Measurement (ARM) program. There is a good correlation (~0.7) between a lidar-derived growth factor (measured over the range 85% RH to 96% RH) with a nephelometer-derived growth factor measured over the RH range 40% to 85%. For these RH ranges, the slope of the lidar-derived growth curve is much steeper than that of the nephelometer-derived growth curve, reflecting the rapid increase in particle size with increasing RH. The results are corroborated by aerosol model calculations of lidar backscatter and nephelometer equivalent *f*(RH) based on in situ aerosol size and composition measurements during the IOP. It is suggested that the lidar method can provide useful measurements of the dependence of aerosol optical properties on relative humidity and under conditions closer to saturation than can currently be achieved with humidified nephelometers.

Citation: Pahlow, M., G. Feingold, A. Jefferson, E. Andrews, J. A. Ogren, J. Wang, Y.-N. Lee, R. A. Ferrare, and D. D. Turner (2006), Comparison between lidar and nephelometer measurements of aerosol hygroscopicity at the Southern Great Plains Atmospheric Radiation Measurement site, *J. Geophys. Res.*, *111*, D05S15, doi:10.1029/2004JD005646.

1. Introduction

[2] The importance of atmospheric aerosols for the Earth's climate has been widely recognized [e.g., *Charlson et al.*, 1992; *Boucher and Anderson*, 1995; *Vogelmann et al.*, 2003]. They affect solar radiation and hence climate directly by scattering radiation back to space [*Charlson et al.*, 1992], but also indirectly by acting as cloud condensation nuclei [*Twomey*, 1974]. An important factor affecting the role aerosols play in climate change is their hygroscopicity. The swelling of aerosols due to water vapor uptake will enhance their ability to scatter radiation. Numerous studies have investigated the relationship between aerosol scattering and relative humidity RH in terms of the hygroscopic growth factor *f*(RH) using humidified nephelometers. These have been used for airborne or ground-based determination of the growth factor considering a "dry" RH over the range 20%–40% and a "wet" RH up to 90% [e.g., *Covert et al.*, 1972; *McInnes et al.*, 1998; *Kotchenruther et al.*, 1999; *Malm et al.*, 2003]. Humidified Tandem Differential Mobility Analyzers (HTDMAs) allow one to determine aerosol hygroscopicity as a function of particle size, usually for RH up to ~90% [e.g., *McMurry and Stolzenburg*, 1989; *Covert and Heintzenberg*, 1993; *Brechtel and Kreidenweis*, 2000]. The lidar (light detection and ranging) technique provides the opportunity to investigate hygroscopic growth of aerosols beyond this RH range, under ambient atmospheric conditions and without perturbing the sampled air. *Ferrare et al.* [1998] used Raman lidar to simultaneously measure aerosol backscatter and RH in a study that demonstrated the ability of lidar to measure $f(\mathrm{RH})_\beta$ (where β denotes backscatter). *Wulfmeyer and Feingold* [2000] used differential absorption lidar to measure $f(\mathrm{RH})_\beta$ in the regime of high RH up to ~98.5%. More recently *Feingold and Morley* [2003] (henceforth FM) used elastic backscatter lidar data combined with thermodynamic

[1]NOAA Environmental Technology Laboratory, Boulder, Colorado, USA.
[2]Now at Ruhr-Universität Bochum, Bochum, Germany.
[3]NOAA Climate Monitoring and Diagnostics Laboratory, Boulder, Colorado, USA.
[4]Brookhaven National Laboratory, Upton, New York, USA.
[5]NASA Langley Research Center, Hampton, Virginia, USA.
[6]Pacific Northwest National Laboratory, Richland, Washington, USA.

0148-0227/06/2004JD005646$09.00

assumptions of the mixing state of the atmosphere to determine $f(\mathrm{RH})_\beta$ for RH up to ~98.5%. In this paper we make use of this combined lidar-thermodynamic approach to determine backscatter $f(\mathrm{RH})_\beta$ for relative humidities close to saturation and for a broad range of atmospheric aerosol conditions. We apply this method for a much broader range of aerosol conditions than has been done in the past. The analysis by *Wulfmeyer and Feingold* [2000] was limited to a 1-min time period and FM analyzed 30 min worth of data. We also provide first comparisons with a ground-based nephelometer-derived $f(\mathrm{RH})$ and show that there is a strong correlation between these two independently derived growth factors. In addition, we show that there is broad consistency between lidar and nephelometer growth factors and those computed from in situ aerosol size distribution and composition measurements during the IOP.

2. Experiment

[3] The data used for our analysis were collected between 1998 and 2003 during both routine measurement periods and the intensive operations period (IOP) in May 2003, at the Southern Great Plains (SGP) Climate Research Facility (CRF) in Oklahoma, USA (latitude +36.605, longitude −97.489; elevation: 315 m asl), as part of the Atmospheric Radiation Measurement (ARM) program. We utilize CRF Raman lidar data (355 nm), three wavelength (450 nm, 550 nm and 700 nm) nephelometer data (two TSI models 3563, one of them humidified, called a humidograph, sampling aerosol particles with a diameter of $\leq$10 μm), light absorption photometer data (Radiance Research model PSAP) adjusted to 550 nm by calibration corrections, as well as micrometeorological data. During the IOP we also use data from a differential mobility analyzer (DMA; TSI model 3081), tapered element oscillating microbalance (TEOM; Rupprecht and Patashnick Series 1400a) and a particle-into-liquid sampler with ion chromatography analysis (PILS-IC [*Orsini et al.*, 2003]). The Raman lidar is a self-contained, fully computer automated system designed for unattended, continuous vertical profiling of water vapor, aerosols and clouds at the ARM SGP CRF [*Goldsmith et al.*, 1998; *Turner et al.*, 2002]. The light source is a frequency-tripled Nd:YAG laser, operating at 30 Hz with 400 mJ pulses to transmit light at 355 nm. The vertical range resolution is 39 m and the time resolution is 10 min, after averaging. Note that the Raman method enables direct measurement of extinction so that in principle, one could measure an extinction-based $f(\mathrm{RH})$. However, in practice, extinction is derived from backscatter below 800 m [*Turner et al.*, 2002], and since this is the region that constitutes a significant fraction of the subcloud region, we use backscatter in our analysis.

[4] The light scattering (nephelometer) and absorption (light absorption photometer) measurements used here are 1-hour averages. The humidograph data were collected over a ~1-hour period, during which the RH was increased from ~30% to ~85%. The DMA samples at 2-min intervals covered a particle size range from 27 nm to 815 nm. TEOM and PILS-IC were measured over 8 min-intervals and interpolated to 5-min intervals. All of these aerosol measurements were made at the surface. Supporting micrometeorological data (potential temperature θ and water vapor mixing ratio r) were collected at 1-min intervals on a tower at a height of 60 m above ground level.

3. Method

[5] To determine a growth factor $f(\mathrm{RH})_\beta$ from Raman lidar backscatter profiles and micrometeorological in situ data we employ thermodynamic assumptions for a cloud-capped, well-mixed boundary layer suggested by FM. For the approach to be applicable, the boundary layer must be well mixed in potential temperature θ, water vapor mixing ratio r, and aerosol. When these criteria are met, the enhancement in backscatter with increasing vertical range is due to water vapor uptake, rather than to the existence of layers of aerosol or poorly defined RH. It is assumed that cloud base z_{cb} corresponds to 100% RH. Using an iterative procedure, the vertical profile of RH can be computed starting from the in situ measurement of θ and r at $z = 60$ m in the following way. Successive height levels z_i are computed according to the hypsometric equation [*Dutton*, 1976, p. 64]

$$z_{i+1} = z_i + R_d \frac{T_v(z_i)}{g} \ln\left[\frac{p(z_i) + dp}{p(z_i)}\right], \tag{1}$$

where R_d is the gas constant of dry air, $T_v(z)$ is the virtual temperature (computed from θ and r, which are assumed to be constant with height), g is acceleration due to gravity, $p(z)$ is atmospheric pressure and dp is a sufficiently small pressure increment to capture cloud base with high accuracy. For each z the RH is determined by

$$\mathrm{RH}(z) = \frac{r(z)}{r_s(T)}, \tag{2}$$

where the saturation water vapor mixing ratio is defined as

$$r_s(T) = \frac{0.622 e_s(T)}{p(z) - e_s(T)} \tag{3}$$

and the saturation vapor pressure $e_s(T)$ is computed according to Magnus' formula [*Iribarne and Godson*, 1973, p. 63]. The iterative procedure is carried out until $r = r_s(T)$, i.e., until cloud base is reached.

[6] Combining the RH(z) profiles from the thermodynamic approach with profiles of the backscatter coefficient β(z) from the Raman lidar enables one to calculate

$$f(\mathrm{RH})_\beta = \beta(\mathrm{RH})/\beta(\mathrm{RH}_{ref}) \tag{4}$$

which expresses the aerosol growth factor in terms of lidar backscatter at a given RH, relative to that at some lower RH_{ref}. Two and three parameter fits $\beta(\mathrm{RH})/\beta(\mathrm{RH_{ref}}) = a[1 - (\mathrm{RH}/100)]^{-b}$ [*Kasten*, 1969] and $\beta(\mathrm{RH})/\beta(\mathrm{RH_{ref}}) = a[1 + b(\mathrm{RH}/100)^c]$ [*Kotchenruther and Hobbs*, 1998], respectively, are applied to the data. We select either the two or three parameter fit according to which provides the best χ^2 goodness of fit. The fit allows us to determine $f(\mathrm{RH})_\beta$ for specific RH values. Similarly these fit equations are also used to determine nephelometer $f(\mathrm{RH})_{neph}$.

[7] To apply the method, the data set was first searched for cloud-capped, well-mixed cases. In order to determine

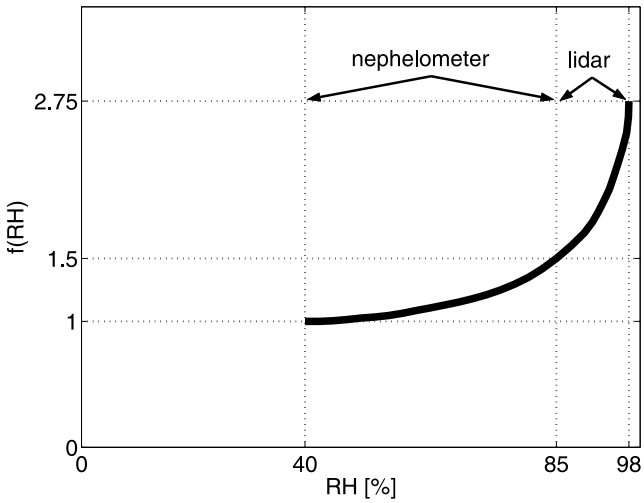

Figure 1. Schematic illustrating the measurement range of nephelometer and lidar and the enhancement in scattering that aerosol undergoes for each respective RH range.

whether the boundary layer was well mixed we inspected the closest (in time) available θ and r profiles from radiosoundings. Furthermore, for the cases selected, it was ascertained that the θ and r measurements at z = 60 m were obtained above the surface layer and in the mixed layer. An additional data selection criterion was the accuracy of the cloud base determination using thermodynamic assumptions, the measure of cloud base used in this study, relative to the cloud base observed by the lidar. The rather coarse lidar range resolution of 39 m renders it unreliable as the sole measure of cloud base and prompted us to investigate more closely the characteristics of cloud base as observed by lidar. Calculations with a one-dimensional parcel model simulating the growth of a population of aerosol particles in an updraft were performed (see FM), and it was shown that the thermodynamically defined cloud base (100% RH) lies in the first one third of the region between the two points in the β(z) profile that exhibit the strongest gradient. Therefore an additional selection criterion for the well-mixed cases was that the thermodynamically derived cloud base did lie within this abovementioned region. This was particularly important when radiosoundings were not temporally close. Time periods that met all the requirements were used for further analysis.

[8] The nephelometer data $f(\mathrm{RH})_{neph}$ and other in situ measurements with which we will be comparing $f(\mathrm{RH})_{\beta}$, were all acquired at the surface. Although the study focuses on well-mixed boundary layers, an a priori requirement for the lidar method to work, there exists a possibility that for different atmospheric stability regimes in the surface layer, the aerosol measured therein might not be representative of the aerosol in the mixed layer aloft. This should be borne in mind in the subsequent discussion (see section 5).

4. Results

4.1. Lidar and Nephelometer *f*(RH)

[9] A total number of 17 lidar time series (3 of which were measured during the IOP) ranging from 10 min to 1 hour met the selection criteria and qualified for the comparison with nephelometer data. It should be noted that the data analyzed here were drawn from a subset of the entire 1998–2003 data set, used for a separate aerosol indirect effect study, and do not reflect the total number of cases during this time period. Figure 1 illustrates that nephelometer and lidar data are complementary for typical RH measurement ranges. Nephelometry measures f(RH) for RH up to 85% and lidar extends the measurement range from 85% RH to close to saturation, i.e., beyond that which can currently be achieved with nephelometry. To compare lidar and nephelometer-derived f(RH) we first determine $f(\mathrm{RH})_{\beta}$ profiles for all 17 cases from the lidar backscatter data and the RH profiles, obtained from the thermodynamic assumptions (Figure 2). The backscatter data are normalized to β(84%–86% RH) (measurements of β are not always available at precisely 85%; for brevity we refer to this range as 85% RH) and the profiles are computed up to RH = 98%. Note the large range of $f(\mathrm{RH})_{\beta}$ values at 98% RH (∼1.5–4.2), for the 17 cases under consideration. Backscatter data obtained at RH > 98% are not considered here because as RH approaches saturation even a small error in the determination of cloud base translates to a large error in RH and hence in $f(\mathrm{RH})_{\beta}$. For example, an error of ±10 m in z_{cb}, results in an error in $f(\mathrm{RH})_{\beta}$ of ±∼12% at RH = 96.5% and ±∼50% at 98.9% RH (FM).

[10] For comparison with nephelometer-derived $f(\mathrm{RH})_{neph}$ for 85%/40% RH and at a wavelength of 450 nm we use the parameters for the fit to the lidar data (at 355 nm) up to 90%, 96% and 98% RH. We account for the different RH measurement ranges of the lidar and the nephelometer by normalizing the growth factors by their respective ranges, ΔRH. (The wavelength difference is discussed in section 5.) Figure 3 shows the comparison between $f(\mathrm{RH})_{neph}$ (85%/40%)/$\Delta\mathrm{RH}_{neph}$ (hereafter referred to as $f(\mathrm{RH})'_{neph}$) and $f(\mathrm{RH})_{\beta}$(90%/85%)/$\Delta\mathrm{RH}_{\beta}$ and indicates no correlation (cor-

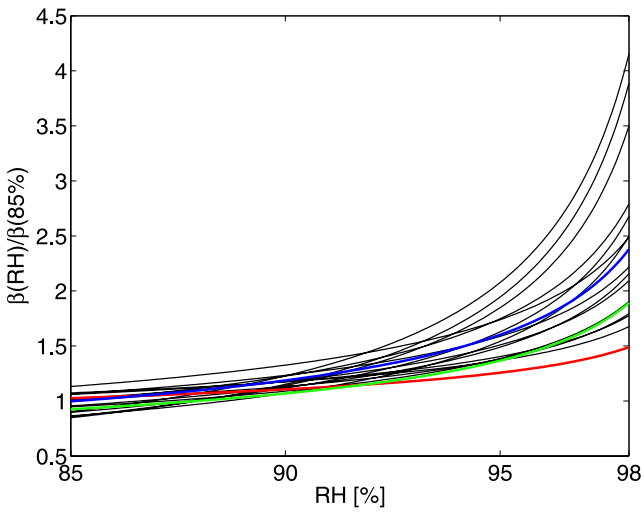

Figure 2. Model parameter fit of $f(\mathrm{RH})_{\beta}$(=β(RH)/β(85%)) to experimental data for RH ranging from 85% to 98%. The 17 cases that were available for analysis are shown. Routine measurement period data are shown as black lines and the IOP data are color coded (red: 8 May; green: 13 May; blue: 17 May).

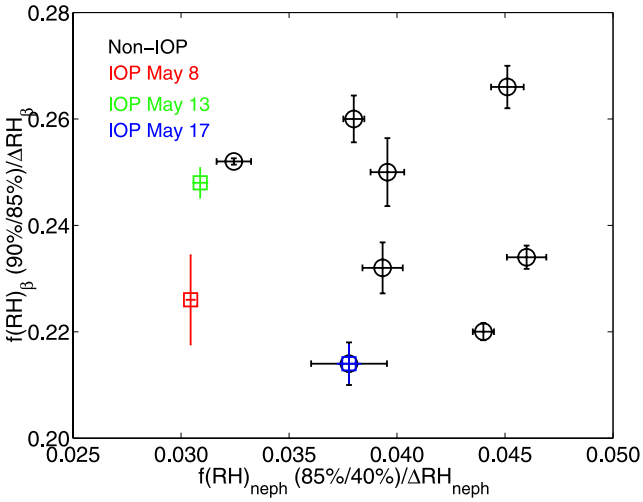

Figure 3. Comparison of the normalized $f(RH)_\beta(90\%/85\%)/\Delta RH_\beta$ (where ΔRH_β = 5%) with $f(RH)_{neph}(85\%/40\%)/\Delta RH_{neph}$ (where ΔRH_{neph} = 45%). Circles denote data obtained during the routine measurement period, and squares represent data obtained during the IOP (red: 8 May; green: 13 May; blue: 17 May). Error bars denote one standard deviation between the measured $f(RH)$ and the $f(RH)$ determined from the fit parameters.

relation coefficient R = 0.02) between normalized lidar and nephelometer derived $f(RH)$ for these RH ranges (humidograph data were available for 11 out of the 17 cases). For an upper limit in RH of 96%, $f(RH)_\beta(96\%/85\%)/\Delta RH_\beta$ correlates well with $f(RH)'_{neph}$ (R = 0.73), as shown in Figure 4. We note that the values of $f(RH)_\beta(96\%/85\%)/\Delta RH_\beta$ are significantly larger than those of $f(RH)'_{neph}$, reflecting the

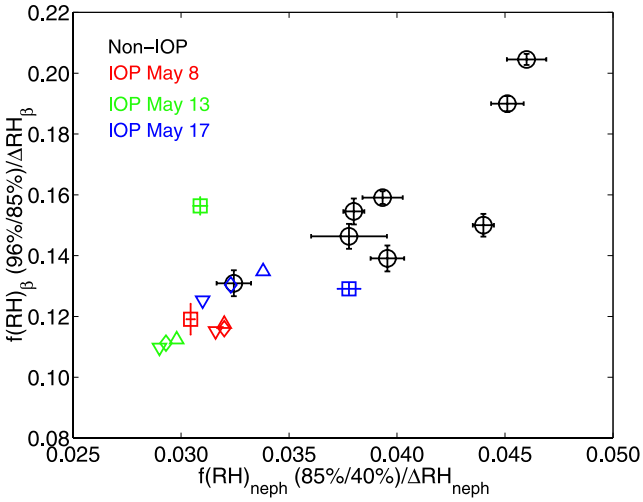

Figure 4. Comparison of the normalized $f(RH)_\beta(96\%/85\%)/\Delta RH_\beta$ (where ΔRH_β = 11%) with $f(RH)_{neph}(85\%/40\%)/\Delta RH_{neph}$. Symbols and error bars are as in Figure 3. Additional symbols represent data computed with an aerosol model. Diamonds represent results obtained for mean inorganic fraction. Upward (downward) pointing triangles were obtained for maximum (minimum) inorganic fraction during the period of interest.

nonlinear increase in growth with increasing RH as illustrated in Figure 1. In Figure 5 $f(RH)'_{neph}$ is compared to $f(RH)_\beta(98\%/85\%)/\Delta RH_\beta$, with a correlation coefficient R = 0.68. This shows that the lidar data contain hygroscopic growth information at increasingly larger RH, and over RH ranges that correspond to significant growth. We stress again that the confidence in the derived $f(RH)_\beta$ decreases as RH approaches saturation but this does not change the qualitative picture that emerges from Figures 3–5.

4.2. Calculations Based on in Situ Aerosol Data

[11] To examine the factors controlling the relationship between lidar and nephelometer derived $f(RH)$ we analyze aerosol size and composition measurements from the DMA, TEOM and PILS-IC for the three days during the IOP that were deemed appropriate for this exercise. Figure 6 shows the mean aerosol size distributions (weighted by surface area) for 8, 13 and 17 May measured by the DMA during the time periods that correspond to the lidar and nephelometer measurements of $f(RH)$. Superimposed on Figure 6 is the scattering efficiency Q_{scat} at 450 nm for an aerosol with negligible absorption. The convolution of the surface size distribution with Q_{scat} represents the contribution of particles of different sizes to the total scattering. We interpolated the measured size distributions onto a finer grid to make them more suitable for model calculations as the Mie calculations behave nonmonotonically with RH if the computational grid is too coarse. Figure 7 shows the aerosol mass concentration C for 8, 13 and 17 May in terms of mean total mass (TEOM), mean inorganic mass (PILS-IC), and the difference between the two; also shown is the mean inorganic fraction which we refer to as ϵ. We use the aerosol size distribution in an aerosol model (FM) to compute backscatter β and total scattering σ_{sp} as a function of RH, thus allowing us to determine lidar and nephelometer-equivalent $f(RH)$. The aerosol model assumes a sulfate, soot and dust mixture with proportions constrained by the measured inorganic fraction ϵ and the measured single scattering albedo ω_o. Without knowledge of the noninorganic aerosol, we make a rough approximation that it is

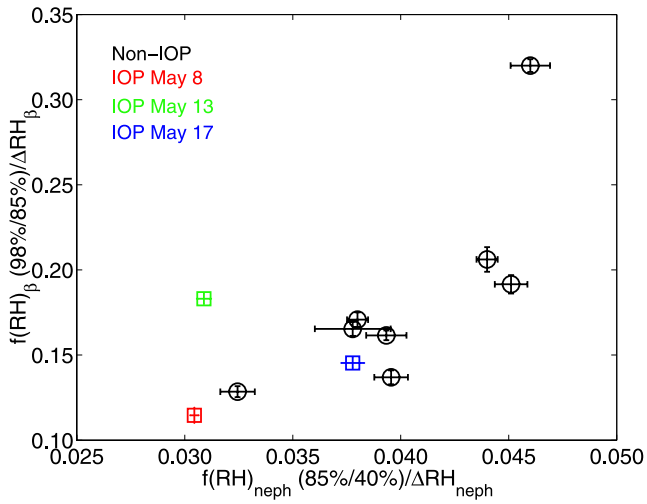

Figure 5. Comparison of the normalized $f(RH)_\beta(98\%/85\%)/\Delta RH_\beta$ (where ΔRH_β = 13%) with $f(RH)_{neph}(85\%/40\%)/\Delta RH_{neph}$. Symbols and error bars are as in Figure 3.

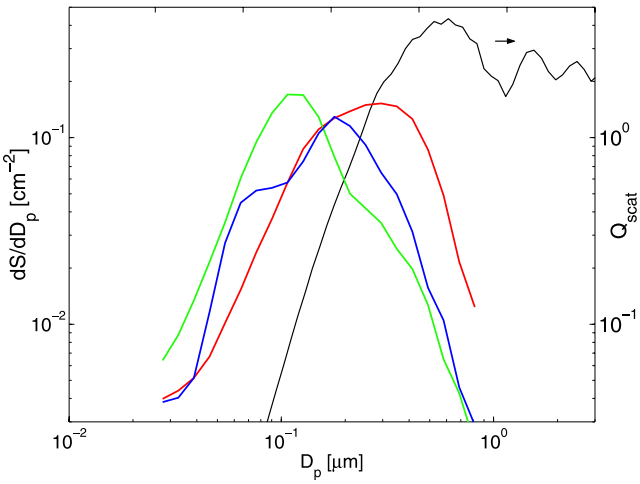

Figure 6. Mean surface size distributions measured on 8 May (red), 13 May (green), and 17 May (blue) during time periods that correspond to the lidar and nephelometer measurement periods (8 May, 1510–1550 UT; 13 May, 1620–1650 UT; and 17 May, 1810–1830 UT). The black line represents the scattering efficiency Q_{scat} at 450 nm for a nonabsorbing aerosol.

insoluble, i.e., that ϵ represents the soluble mass fraction. We then perform calculations with a range of ϵ values to account for the likelihood that some of the noninorganic fraction is soluble.

[12] The normalized growth factors, as computed from the in situ size distribution and composition data for 8, 13 and 17 May, are superimposed as colored symbols in Figure 4. For this comparison we focus on the relationship between $f(\mathrm{RH})_\beta(96\%/85\%)/\Delta\mathrm{RH}_\beta$ (hereafter termed $f(\mathrm{RH})'_\beta$) and $f(\mathrm{RH})'_{neph}$, as we have more confidence in the data from this RH range, and because the correlation between the lidar and nephelometer is the greatest. On 8 May the normalized measured lidar and nephelometer f(RH) compare well with the normalized f(RH) computed from the in situ data. As noted above, the fraction of soluble material is uncertain and so the mean values are perturbed to the minimum and maximum values observed during the time period. These variations in ϵ have the effect of increasing (decreasing) both the lidar and nephelometer equivalent f(RH) values for increasing (decreasing) ϵ (Figure 4) but their positions do not deviate very much from the general trend because changes in ϵ affect particle scattering and backscatter to similar degrees.

[13] In Figure 8 both the normalized lidar backscatter (β_{norm}) and normalized nephelometer total scattering σ_{norm} from measurements (circles) and the aerosol model calculations (stars) are shown. As before, nephelometer total scattering coefficients are calculated with respect to the 40% RH total scattering coefficient whereas the lidar backscatter coefficients are calculated with respect to β(85% RH). Small disagreements in σ_{norm} at 40% RH are associated with slightly different normalization procedures between nephelometer measurements and the calculations based on in situ aerosol measurements. For this reason, only the slopes of σ_{norm} should be compared. Both measured and computed β_{norm} and σ_{norm} profiles show similar slopes for 8 May, hence the proximity between the red square and red diamond in the $f(\mathrm{RH})'_\beta$ versus $f(\mathrm{RH})'_{neph}$ (Figure 4). On 13 May the normalized f(RH) computed from in situ data compares well with the measured nephelometer $f(\mathrm{RH})'_{neph}$, but it differs from the measured lidar $f(\mathrm{RH})'_\beta$. This is reflected in Figure 4 by close proximity between green square and green diamond in nephelometer scattering space (x-axis) but disagreement in lidar backscatter space (y-axis). Figure 8 clearly shows the steeper slope in the measured profile of β_{norm} when compared to β_{norm} computed from in situ data. We suspect that the arrival of a frontal passage might have caused the discrepancy between values measured with lidar and computed from in situ data. Figures 9a

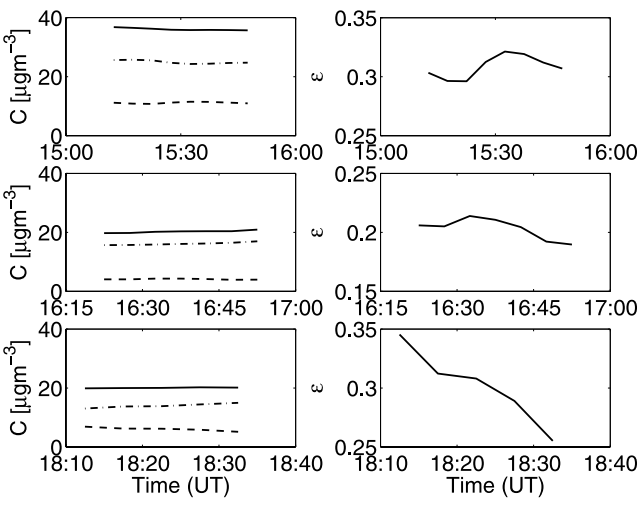

Figure 7. (left) Aerosol composition C in terms of total mass (solid line), inorganic fraction (dashed line) and the difference between the two (dashed-dotted line); (right) inorganic fraction ϵ; (top) 8 May, (middle) 13 May, and (bottom) 17 May.

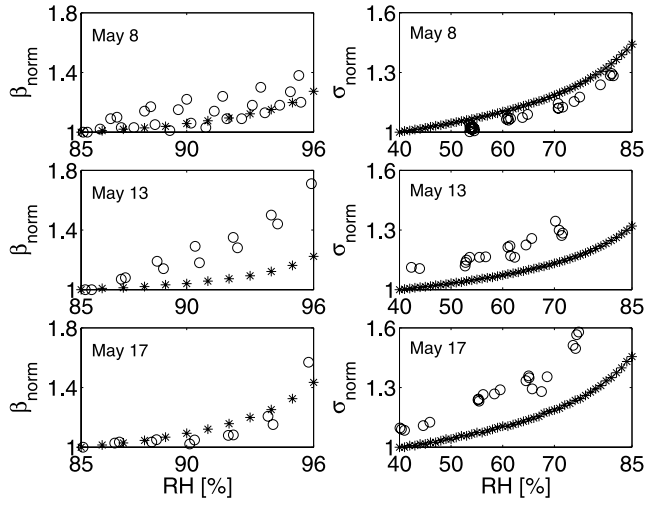

Figure 8. Normalized measured lidar and nephelometer backscatter and total scattering coefficients (circles) and normalized computed backscatter and total scattering coefficients from aerosol model (stars). (left) Normalized backscatter coefficients β_{norm} and (right) normalized total scattering coefficients σ_{norm}.

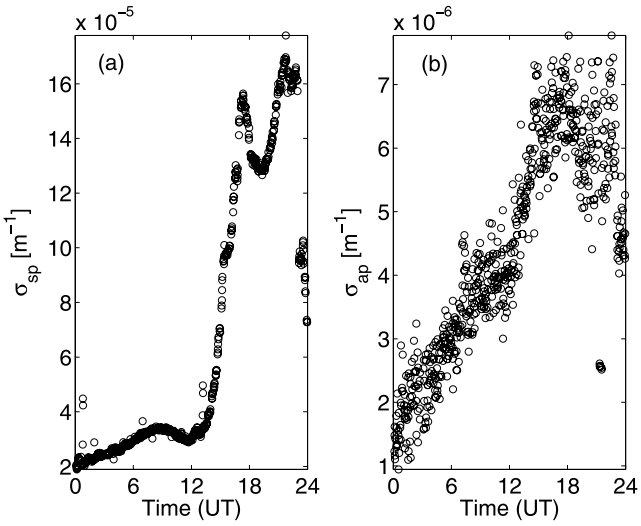

Figure 9. Time series of (a) total scattering coefficient σ_{sp} at 450 nm and (b) absorption coefficient σ_{ap} at 565 nm for 13 May.

and 9b show the measured time series of the total scattering coefficient σ_{sp} and absorption coefficient σ_{ap}, respectively. Figures 9a and 9b indicate a rapid change in aerosol size and composition starting at ~1320 UT until ~1720 UT, which encompasses the lidar and nephelometer measurement period from 1620 to 1650 UT. Because of this rapid change in aerosol properties, the surface layer and the mixed layer aerosol might have differed substantially, which could have contributed to the difference in $f(\mathrm{RH})'_{\beta}$ and $f(\mathrm{RH})'_{neph}$. On 17 May the measured lidar $f(\mathrm{RH})'_{\beta}$ and the computed $f(\mathrm{RH})'_{\beta}$ compare well, however, the slopes for the measured and computed normalized nephelometer scattering coefficients differ (Figure 8). This is reflected in Figure 4 by agreement between blue square and blue diamond in lidar backscatter space (y-axis) but disagreement in nephelometer space (x-axis). The source of this disagreement is unresolved.

4.3. *f*(RH), *å* and ω_o

[14] As this data set covers a broad range of atmospheric aerosol conditions (Figure 2) it is instructive to investigate the relationship between *f*(RH) and the Ångström exponent *å*, a parameter closely related to the size distribution of the aerosol population. In 14 of the 17 cases studied here nephelometer data at 450 nm and 700 nm were available to compute *å*. In Figure 10, $f(\mathrm{RH})'_{\beta}$ (which is qualitatively similar to $f(\mathrm{RH})'_{neph}$; Figure 4) is plotted against *å*. The data indicate that $f(\mathrm{RH})'_{\beta}$ tends to increase with increasing *å* although the correlation is weak (R = 0.15). This qualitative trend can be explained by the fact that at large *å*, there is a preponderance of small particles with low scattering efficiency. The effect of increasing RH is to allow these particles to grow to sizes at which they are more efficient scatterers. *Sheridan et al.* [2001] found, on the basis of analysis of in situ data collected at SGP in 1999, that aerosols containing higher fractions of smaller particles show larger hygroscopic growth factors. This is consistent with the trend for $f(\mathrm{RH})'_{\beta}$ versus *å* found here.

[15] It is likely that *f*(RH) is closely tied to aerosol composition. For example, the water vapor uptake by inorganic salts is typically higher than for dicarboxylic organic acids [*Saxena and Hildemann*, 1996]. Also, mixtures of inorganic and organic material may exhibit suppressed deliquescence relative humidity [*Raymond and Pandis*, 2002]. Since for non-IOP days complete aerosol composition data are unavailable, and because we expect the amount of organic material (particularly black carbon) to affect both water vapor uptake and light absorption, we use the single scattering albedo ω_o as a composition proxy to explore the effect of composition on *f*(RH). In Figure 11 $f(\mathrm{RH})'_{\beta}$ is plotted as a function of ω_o for 8 out of a total of 17 cases that were available (only a limited number of absorption measurements, required for the determination of ω_o, was available because of instrument downtime). The range of ω_o is 0.922 to 0.980. The data show a weak positive correlation (R = 0.43), but because of the sparseness of the data a clear trend cannot be deduced. We refer again to the study by *Sheridan et al.* [2001] who showed that aerosols containing higher fractions of more strongly absorbing particles exhibit lower hygroscopic growth factors. *Delene and Ogren* [2002] studied the behavior of ω_o as a function of the aerosol light scattering coefficient for data collected over a three and a half year period at the SGP site. They found that ω_o increased with increasing aerosol light scattering coefficient. However, future studies will be required to clarify the relationship between *f*(RH) and ω_o.

5. Discussion

[16] The consistency between the measurements of $f(\mathrm{RH})'_{\beta}$ and $f(\mathrm{RH})'_{neph}$ described above provides confidence in the lidar methodology for studying aerosol hygroscopic growth. Nevertheless, a number of issues need to be

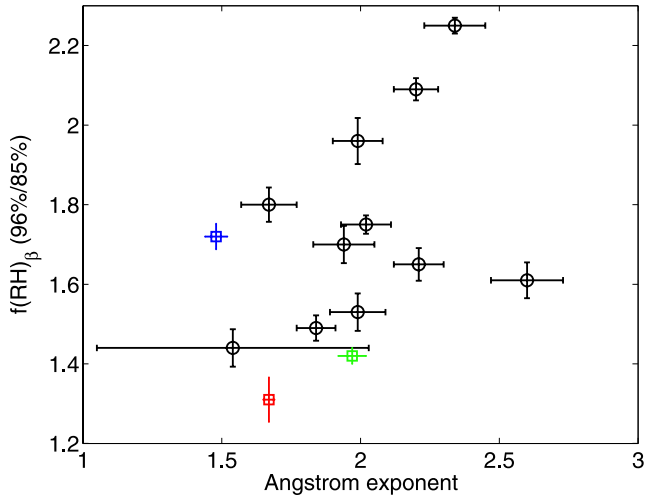

Figure 10. $f(\mathrm{RH})_{\beta}$ (96%/85%) as a function of Ångström exponent *å* as determined from nephelometer at 700 nm and 450 nm. The error bars for *å* represent one standard deviation from the mean in *å* over the respective measurement period. Error bars for $f(\mathrm{RH})_{\beta}$ (96%/85%) denote one standard deviation between the measured $f(\mathrm{RH})_{\beta}$ and the $f(\mathrm{RH})_{\beta}$ determined from the fit parameters. Symbols are as in Figure 3.

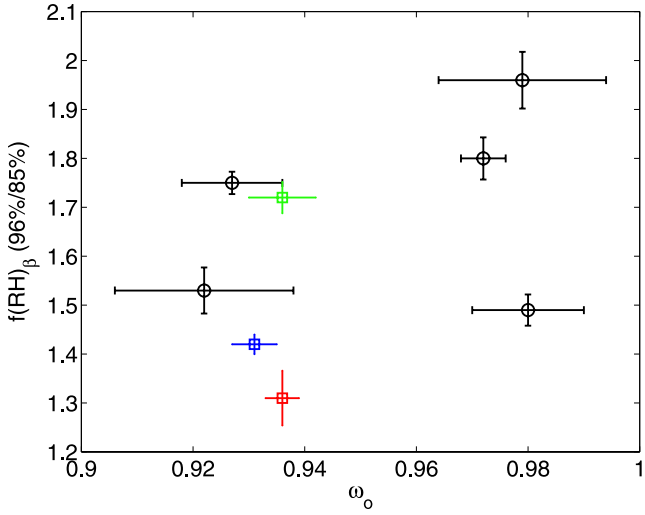

Figure 11. $f(\mathrm{RH})_\beta(96\%/85\%)$ as a function of single scattering albedo ω_o as determined from the nephelometer at 450 nm and the light absorption photometer. The error bars for ω_o represent one standard deviation from the mean in ω_o over the respective measurement period. Error bars for $f(\mathrm{RH})_\beta(96\%/85\%)$ denote one standard deviation between the measured $f(\mathrm{RH})_\beta$ and the $f(\mathrm{RH})_\beta$ determined from the fit parameters. Symbols are as in Figure 3.

factored in to these comparisons. The importance of these will vary depending on the particular aerosol conditions that present themselves. The following important caveats should be considered:

[17] 1. A lidar measures 180° backscatter whereas a nephelometer measures total scattering. FM addressed this issue and showed with model calculations for marine type aerosol that for RH < ~95%, $f(\mathrm{RH})_\beta \simeq f(\mathrm{RH})_{neph}$. However, the agreement may vary for different aerosol size distribution and composition.

[18] 2. The two instruments measure over different RH ranges. We note that the general relationship between $f(\mathrm{RH})'_\beta$ and $f(\mathrm{RH})'_{neph}$ is closely related to the selected RH ranges for each instrument. Nephelometer $f(\mathrm{RH})$ is commonly computed over a RH range from 40% to 85% and this convention has been adopted here. In the case of lidar we investigate three RH ranges to compute $f(\mathrm{RH})'_\beta$ (90%, 96% and 98%) and find good correlation with $f(\mathrm{RH})'_{neph}$ for both upper limits 96% and 98%.

[19] 3. The lidar measures at 355 nm whereas the nephelometer measures at 450 nm. From model calculations we find that the effect of the wavelength difference on backscatter and total scattering is closely related to the aerosol size distribution and composition. On the basis of extensive calculations (not shown) we draw the following broad generalizations: (1) The more absorbing the particles, the larger the total scattering relative to the backscatter (and hence the larger $f(\mathrm{RH})_{neph}$ relative to $f(\mathrm{RH})_\beta$); (2) the difference between backscatter and total scattering due to the wavelength difference tends to be less significant for smaller particles. For a more quantitative assessment, these biases should be considered on a case-by-case basis.

[20] 4. $f(\mathrm{RH})_\beta$ is based on lidar profiling of the mixed layer, whereas $f(\mathrm{RH})_{neph}$ is determined from in situ ground based measurements in the surface layer. The surface layer is in general affected by surface processes on shorter timescales than the mixed layer. Apparently this did not significantly affect the current analysis except for the IOP day 13 May when the arrival of a frontal passage may have resulted in different aerosol properties within the surface layer and in the mixed layer. The fact that time-averaged quantities were used rather than instantaneous measurements may have alleviated this problem. In situ aerosol measurements on the 60 m tower would have been desirable, although impractical. Alternatively, a scanning lidar would have enabled the lidar to sample the aerosol in the surface layer. One might speculate that were such measurements available, the correlation between $f(\mathrm{RH})_\beta$ and $f(\mathrm{RH})_{neph}$ might have been even higher.

[21] 5. Cloud base height has been determined here on the basis of thermodynamic arguments rather than from lidar backscatter, as the Raman lidar range resolution is too coarse for this purpose. To obtain high accuracy in cloud base determination using thermodynamic arguments it is important that the micrometeorological parameters be measured in the mixed layer, as was done here. Ideally, however, a lidar with high spatial resolution (order of meters) should be used as an additional measure of cloud base (see FM). Furthermore, combined Raman lidar and Atmospheric Emitted Radiance Interferometer (AERI) and Geostationary Operational Environmental Satellite (GOES) measurements of RH [*Turner et al.*, 2000] could be included in future analyses. Comparison between lidar-derived and thermodynamically derived cloud base will provide a stronger criterion for well-mixed conditions and provide greater confidence in $f(\mathrm{RH})_\beta$ at RH close to saturation.

6. Summary

[22] A lidar technique that employs thermodynamic assumptions for well-mixed, cloud-capped boundary layers has been used to compute profiles of the hygroscopic growth factor $f(\mathrm{RH})$ for ambient, unperturbed atmospheric conditions. The lidar-derived backscatter $f(\mathrm{RH})$ over the range 85% to 96% RH correlates well with the growth factors from a collocated ground-based humidified nephelometer (40% RH to 85% RH). To our knowledge, this is the first observational evidence of the consistency between these two measures of $f(\mathrm{RH})$. The slopes of the growth curves reflect the fact that the growth over the range 85% RH to 96% RH is much stronger than over the range 40% to 85%. The measurements were corroborated by a comparison of measured $f(\mathrm{RH})$ with those computed from in situ measurement of size distribution and composition for three cases during the May 2003 IOP.

[23] We have investigated the possible relationship between aerosol size distribution and $f(\mathrm{RH})_\beta$ using the Ångström exponent as a proxy for size distribution. The data suggest that $f(\mathrm{RH})_\beta(96\%/85\%)$ increases with increasing *å*. A plausible explanation is that at high *å*, the dominance of smaller particles that are inefficient scatterers yields low backscatter, and their growth due to uptake of water vapor allows them to scatter more efficiently. At low å, the growth of the larger particles, that are already efficient scatterers, has less effect on $f(\mathrm{RH})_\beta$. Preliminary investigation of the effect of aerosol composition (represented by the single-

scattering albedo) shows a weak positive trend between $f(\mathrm{RH})_\beta$(96%/85%) and ω_o, but because of the rather small number of data points analyzed, we cannot draw any conclusions regarding the suitability of ω_o as a proxy for aerosol composition. Further analyses are required to determine whether there is a clear relationship between $f(\mathrm{RH})_\beta$ and ω_o.

[24] The current study extends the prior demonstrations of this technique by *Wulfmeyer and Feingold* [2000] and FM and provides further confidence that lidar can be a useful tool for measurement of aerosol growth, particularly at RH >85%. It is suggested that measurements of this kind will benefit greatly from higher lidar range resolution (on the order of meters) which will increase the accuracy of retrievals at RH approaching saturation. Recent upgrades to the CRF Raman lidar [*Turner and Goldsmith*, 2005] to a range resolution of 7.5 m will greatly assist in this regard.

[25] **Acknowledgments.** The data used for this study were obtained from the Atmospheric Radiation Measurement (ARM) Program sponsored by the U.S. Department of Energy, Environmental Sciences Division. The authors thank the awarding agency as well as ARM staff for maintaining the instrumentation and the ARM database. We acknowledge the role of ARM's Climate Research Facility in supporting the acquisition of surface aerosol data. M.P. was supported by the NOAA Postdoctoral Program in Climate and Global Change, administered by the University Corporation for Atmospheric Research. G.F. was supported by the Biological and Environmental Research program (BER), U.S. Department of Energy, grant DE-A103-02ER63324, and by NOAA's Climate and Global Change Program.

References

Boucher, O., and T. L. Anderson (1995), General circulation model assessment of the sensitivity of direct climate forcing by anthropogenic sulfate aerosols to aerosol size and chemistry, *J. Geophys. Res.*, *100*, 26,117–26,134.

Brechtel, F. J., and S. M. Kreidenweis (2000), Predicting particle critical supersaturation from hygroscopic growth measurements in the humidified TDMA. part II: Laboratory and ambient studies, *J. Atmos. Sci.*, *57*, 1872–1887.

Charlson, R. J., S. E. Schwartz, J. M. Hales, R. D. Cess, J. A. Oakley Jr., J. E. Hansen, and D. J. Hofmann (1992), Climate forcing by anthropogenic aerosols, *Science*, *255*, 423–430.

Covert, D. S., and J. Heintzenberg (1993), Size distribution and chemical properties of aerosol at Ny Alesund, Svalbard, *Atmos. Environ., Part A*, *27*, 2989–2997.

Covert, D. S., R. J. Charlson, and N. C. Ahlquist (1972), A study of the relationship of chemical composition and humidity to light scattering by aerosols, *J. Appl. Meteorol.*, *11*, 968–976.

Delene, D. J., and J. A. Ogren (2002), Variability of aerosol optical properties at four North American surface monitoring sites, *J. Atmos. Sci.*, *59*, 1135–1150.

Dutton, J. A. (1976), *Dynamics of Atmospheric Motion*, 617 pp., Dover, Mineola, N. Y.

Feingold, G., and B. Morley (2003), Aerosol hygroscopic properties as measured by lidar and comparison with in situ measurements, *J. Geophys. Res.*, *108*(D11), 4327, doi:10.1029/2002JD002842.

Ferrare, R. A., S. H. Melfi, D. N. Whiteman, K. D. Evans, M. Poellot, and Y. J. Kaufman (1998), Raman lidar measurements of aerosol extinction and backscattering: 2. Derivation of aerosol real refractive index, single-scattering albedo, and humidification factor using Raman lidar and aircraft size distribution measurements, *J. Geophys. Res.*, *103*, 19,673–19,689.

Goldsmith, J. E. M., S. E. Bisson, H. B. Blair, and D. D. Turner (1998), Turn-key Raman lidar for profiling atmospheric water vapor, clouds, and aerosols, *Appl. Opt.*, *37*, 4979–4990.

Iribarne, J. V., and W. L. Godson (1973), *Atmospheric Thermodynamics*, 222 pp., Springer, New York.

Kasten, F. (1969), Visibility forecast in the phase of pre-condensation, *Tellus*, *21*, 631–635.

Kotchenruther, R. A., and P. V. Hobbs (1998), Humidification factors of aerosols from biomass burning in Brazil, *J. Geophys. Res.*, *103*, 32,081–32,089.

Kotchenruther, R. A., P. V. Hobbs, and D. A. Hegg (1999), Humidification factors for atmospheric aerosols off the mid-Atlantic coast of the United States, *J. Geophys. Res.*, *104*, 2239–2251.

Malm, W. C., D. E. Day, S. M. Kreidenweis, J. L. Collett, and T. Lee (2003), Humidity-dependent optical properties of fine particles during the Big Bend Regional Aerosol and Visibility Observational Study, *J. Geophys. Res.*, *108*(D9), 4279, doi:10.1029/2002JD002998.

McInnes, L., M. Bergin, J. Ogren, and S. Schwartz (1998), Apportionment of light scattering and hygroscopic growth to aerosol composition, *Geophys. Res. Lett.*, *25*, 513–516.

McMurry, P. H., and M. R. Stolzenburg (1989), On the sensitivity of particle size to relative humidity for Los Angeles aerosols, *Atmos. Environ.*, *23*, 497–507.

Orsini, D. A., Y. Ma, A. Sullivan, B. Sierau, K. Baumann, and R. J. Weber (2003), Refinements to the particle-into-liquid sampler (PILS) for ground and airborne measurements of water soluble aerosol composition, *Atmos. Environ.*, *37*, 1243–1259.

Raymond, T. M., and S. N. Pandis (2002), Cloud activation of single-component organic aerosol particles, *J. Geophys. Res.*, *107*(D24), 4787, doi:10.1029/2002JD002159.

Saxena, P., and L. M. Hildemann (1996), Water-soluble organics in atmospheric particles: A critical review of the literature and application of thermodynamics to identify candidate compounds, *J. Atmos. Chem.*, *24*, 57–109.

Sheridan, P. J., D. J. Delene, and J. A. Ogren (2001), Four years of continuous surface aerosol measurements from the Department of Energy's Atmospheric Radiation Measurement Program Southern Great Plains Cloud and Radiation Testbed site, *J. Geophys. Res.*, *106*, 20,735–20,747.

Turner, D. D., and J. E. M. Goldsmith (2005), The refurbishment and upgrade of the Atmospheric Radiation Measurement Raman lidar, paper presented at 15th Atmospheric Radiation Measurement Program Science Team Meeting, U.S. Dep. of Energy, Daytona Beach, Fla. (Available at http://www.arm.gov/publications/proceedings/conf15/extended_abs/turner_dd1.pdf)

Turner, D. D., W. F. Feltz, and R. A. Ferrare (2000), Continuous water vapor profiles from operational ground-based active and passive remote sensors, *Bull. Am. Meteorol. Soc.*, *81*, 1301–1317.

Turner, D. D., R. A. Ferrare, L. A. Heilman, W. F. Feltz, and T. P. Tooman (2002), Automated retrievals of aerosol extinction coefficient from Raman lidar, *J. Atmos. Oceanic Technol.*, *19*, 37–50.

Twomey, S. (1974), Pollution and the planetary albedo, *Atmos. Environ.*, *8*, 1251–1256.

Vogelmann, A. M., P. J. Flatau, M. Szczodrak, K. M. Markowicz, and P. J. Minnett (2003), Observations of large aerosol infrared forcing at the surface, *Geophys. Res. Lett.*, *30*(12), 1655, doi:10.1029/2002GL016829.

Wulfmeyer, V., and G. Feingold (2000), On the relationship between relative humidity and particle backscattering coefficient in the marine boundary layer determined with differential absorption lidar, *J. Geophys. Res.*, *105*, 4729–4741.

E. Andrews, A. Jefferson, and J. A. Ogren, NOAA Climate Monitoring and Diagnostics Laboratory, 325 Broadway, Boulder, CO 80305, USA. (betsy.andrews@noaa.gov; anne.jefferson@noaa.gov; john.a.ogren@noaa.gov)

G. Feingold, NOAA Environmental Technology Laboratory, 325 Broadway, CO 80305, USA. (graham.feingold@noaa.gov)

R. A. Ferrare, NASA Langley Research Center, Hampton, VA 23681, USA. (richard.a.ferrare@nasa.gov)

Y.-N. Lee and J. Wang, Brookhaven National Laboratory, Upton, NY 11973, USA. (ynlee@bnl.gov; jian@bnl.gov)

M. Pahlow, Ruhr-Universität Bochum, Lehrstuhl für Hydrologie, Wasserwirtschaft und Umwelttechnik, D-44780 Bochum, Germany. (markus.pahlow@rub.de)

D. D. Turner, Pacific Northwest National Laboratory, Richland, WA 99352, USA. (dave.turner@pnl.gov)